



Machine-learning methods based on the texture and non-texture features of MRI for the preoperative prediction of sentinel lymph node metastasis in breast cancer

Jian Wang^{1,2,3#}, Xinna Gao^{3#}, Shuixing Zhang^{4,5^}, Yu Zhang^{1,2^}

¹School of Biomedical Engineering, Southern Medical University, Guangzhou, China; ²Guangdong Provincial Key Laboratory of Medical Image Processing, Southern Medical University, Guangzhou, China; ³Department of Radiation Oncology, Nanfang Hospital, Southern Medical University, Guangzhou, China; ⁴Medical Imaging Center, First Affiliated Hospital of Jinan University, Guangzhou, China; ⁵Institute of Molecular and Functional Imaging, Jinan University, Guangzhou, China

Contributions: (I) Conception and design: Y Zhang, S Zhang; (II) Administrative support: Y Zhang, S Zhang; (III) Provision of study materials or patients: S Zhang; (IV) Collection and assembly of data: X Gao; (V) Data analysis and interpretation: J Wang; (VI) Manuscript writing: All authors; (VII) Final approval of manuscript: All authors.

[#]These authors contributed equally to this work as co-first authors.

Correspondence to: Shuixing Zhang, MD. Medical Imaging Center, First Affiliated Hospital of Jinan University, No. 613, Huangpu West Road, Tianhe District, Guangzhou 510627, China; Institute of Molecular and Functional Imaging, Jinan University, Guangzhou, China. Email: shui7515@126.com; Yu Zhang, PhD. School of Biomedical Engineering, Southern Medical University, No. 1838, Guangzhou Northern Avenue, Baiyun District, Guangzhou 510515, China; Guangdong Provincial Key Laboratory of Medical Image Processing, Southern Medical University, Guangzhou, China. Email: yuzhang@smu.edu.cn.

Background: The establishment of an accurate, stable, and non-invasive prediction model of sentinel lymph node (SLN) metastasis in breast cancer is difficult nowadays. The aim of this work is to identify the optimal machine learning model based on the three-dimensional (3D) image features of magnetic resonance imaging (MRI) for the preoperative prediction of SLN metastasis in breast cancer patients.

Methods: A total of 172 patients with histologically proven breast cancer were enrolled retrospectively, including 74 SLN metastasis patients and 98 non-SLN metastasis patients. All of them underwent diffusion-weighted imaging (DWI) magnetic resonance imaging (MRI) scan. Firstly, a total of 10,320 texture and four non-texture features were extracted from the region of interests (ROIs) of image. Twenty-four feature selection methods and 11 classification methods were then evaluated by using 10-fold cross-validation to identify the optimal machine learning model in terms of the mean area under the curve (AUC), accuracy (ACC), and stability.

Results: The result showed that the model based on the combination of minimum redundancy maximum relevance (MRMR) + random forest (RF) exhibited the optimal predictive performance (AUC: 0.97 ± 0.03 ; ACC: 0.89 ± 0.05 ; stability: 2.94). Moreover, we independently investigated the performance of feature selection methods and classification methods, and observed that L^1 -support vector machine (L^1 -SVM) (AUC: 0.80 ± 0.08 ; ACC: 0.76 ± 0.07) and sequential forward floating selection (SFFS) (stability: 3.04) presented the best average predictive performance and stability among all feature selection methods, respectively. RF (AUC: 0.85 ± 0.11 ; ACC: 0.80 ± 0.09) and SVM (stability: 8.43) showed the best average predictive performance and stability among all classification methods, respectively.

Conclusions: The identified model based on the 3D image features of MRI provides a non-invasive way for the preoperative prediction of SLN metastasis in breast cancer patients.

Keywords: Machine learning; magnetic resonance imaging (MRI); breast cancer; sentinel lymph node (SLN); preoperative prediction

[^] ORCID: Shuixing Zhang, 0000-0001-7377-382X; Yu Zhang, 0000-0001-8456-7335.

Submitted Nov 02, 2022. Accepted for publication Oct 24, 2023. Published online Dec 06, 2023.

doi: 10.21037/tcr-22-2534

View this article at: <https://dx.doi.org/10.21037/tcr-22-2534>

Introduction

Breast cancer is the most frequently diagnosed cancer and the leading type of cancer among females worldwide, accounting for 24.5% of newly diagnosed female cancers in 2020 (1). An early diagnosis is key to the successful treatment of breast cancer (1,2). The axillary lymph node (ALN) status, a crucial prognostic factor for breast cancer, guides decision-making regarding treatment modalities (3); thus, the determination of the ALN status is important to the correct staging of breast cancer patients (4,5). The sentinel lymph node (SLN) is the first lymph node that receives lymphatic drainage from the tumor and it can predict the ALN status accurately (6). Therefore, SLN biopsy (SLNB) has been introduced as an alternative method to screening the ALN for metastasis, especially for early-stage breast cancer (7-10). Nevertheless, some work presented the morbidity associated with the invasive SLNB and highlighted the fact that the procedure inevitably has complications (11,12). The accurate non-invasive detection method of SLN metastasis is meaningful. Several studies have reported that clinical and histopathological data provides predictive information for SLN metastasis; but some predictive information is just obtained after operation, thereby failing to guide SLN detection (13-16). Therefore,

a new preoperative method for SLN detection has been proposed based on contrast-enhanced ultrasonography with sonazoid in breast cancer; however, this method has only been applied to a small cohort, and its accuracy (ACC) and practicality remains controversial (17,18).

Medical images, changing rapidly from being primarily a diagnostic tool to playing a key role in precision medicine, providing a feasible non-invasive way to decode tumor pathophysiology by high-throughput extraction of quantitative features that transform visual images into quantifiable information (19). Typically, some studies have reported that the quantitative features derived from medical images are associated with clinical features, including histology, grades or stages of cancer, patient survival, and metastases (20-23). Several papers have explored the potential association between gene expression pattern and quantitative features (24,25). Three steps are involved in this type of analysis: region of interest (ROI) segmentation, feature extraction, and classifier modeling. The segmentation of ROIs is usually performed manually by radiologists, and the auto segmentation is still a challenge due to the indistinct borders of many tumors. The high-throughput extraction of quantitative features is imperative, and image processing technologies have provided a series of feature extraction algorithms for quantizing tumor heterogeneity (26). A high-performance classifier is then required to help making clinical decision. In general, to achieve better classification results, the feature selection approach is employed to reduce the dimension of the features space. Consequently, as a research hotspot, machine learning offers numerous feature selection operators; it is divided into three main categories, namely, filter, wrapper, and embedded methods (27,28). The performance of feature selection is entwined with classification method (29,30).

In this study, we aimed to provide a non-invasive and efficient way to predict SLN metastasis in breast cancer patients. We built a prediction model, which consisted of feature extraction, feature selection and classification modules. *Figure 1* shows the framework of our study. To achieve the optimal combination of feature selection and classification methods, we extensively evaluated different combination of 24 feature selection and 11 classification methods in terms of their average performance and

Highlight box

Key findings

- A non-invasive and efficient prediction model to predict sentinel lymph node (SLN) metastasis based on the image features of magnetic resonance imaging in breast cancer patients was constructed.

What is known and what is new?

- The accurate prediction model can be established using the method of radiomics.
- The prediction model with combination of minimum redundancy maximum relevance and random forest could facilitate clinical prediction of SLN metastasis for patients with breast cancer.

What is the implication, and what should change now?

- More collection of magnetic field inhomogeneity of diffusion-weighted images and more complex machine learning methods should be included in future research.

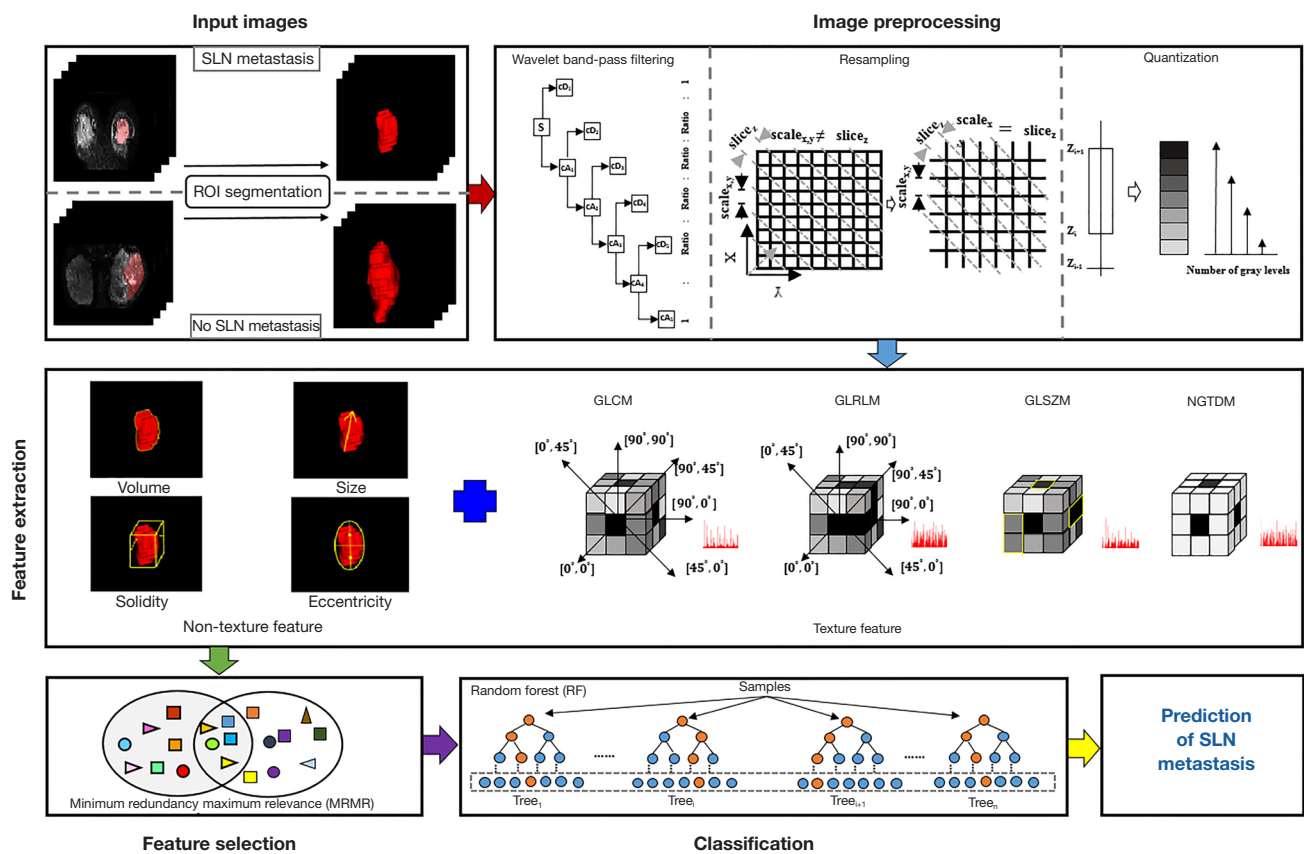


Figure 1 The flowchart of our work in this paper. It mainly refers to three steps, including: (I) ROI segmentation and image preprocessing; (II) non-texture and texture feature extraction; and (III) feature selection and classification. SLN, sentinel lymph node; ROI, region of interest; GLCM, gray-level co-occurrence matrix; GLRLM, gray-level run-length matrix; GLSZM, gray-level size zone matrix; NGTDM, neighborhood gray-tone difference matrix.

stability. Moreover, to explore predictive performance of feature selection and classification method separately, we independently compared feature selection and classification methods. Feature selection and classification methods were independently compared. We present this article in accordance with the TRIPOD reporting checklist (available at <https://tcr.amegroups.com/article/view/10.21037/tcr-22-2534/rc>).

Methods

Patients

This study does not need Institutional Review Board (IRB) approval due to the purpose of retrospective study and was conducted in accordance with the Declaration of Helsinki (as revised in 2013). The individual consent

for this retrospective analysis was waived. A total of 172 patients were retrospectively reviewed from March 2014 to June 2016. SLN metastasis (n=74) and non-SLN metastasis (n=98) in breast cancer patients had been histologically confirmed. All enrolled patients underwent diffusion-weighted imaging (DWI) magnetic resonance imaging (MRI) scan. The baseline characteristics of enrolled patients are listed in *Table 1*. The ROIs were defined as the whole single breast tumor. To reduce the perturbation brought by random dataset partition, motivated by the approach proposed by Haury *et al.* (30), 172 patients were enrolled in total in this work. In order to investigate the stability of feature selection-classification combinations and eliminate the influence of data division, the 172 patients were randomly divided into 50 subsets with 138 patients (80% of the enrolled patients). For each subset, 10-fold cross-

Table 1 The baseline characteristics of enrolled patients

Characteristics	Non-SLN metastasis group (n=98)	SLN metastasis group (n=74)
Age (years)	47.10±11.0	48.0±10.2
Histological grade		
I	14 (14.3)	3 (4.1)
II	35 (35.7)	27 (36.5)
III	42 (42.9)	25 (33.8)
Other	7 (7.1)	19 (25.7)
ER status		
Negative	23 (23.5)	5 (6.8)
1+	14 (14.3)	8 (10.8)
2+	12 (12.2)	10 (13.5)
3+	42 (42.9)	32 (43.2)
Other	7 (7.1)	19 (25.7)
PR status		
Negative	19 (19.4)	5 (6.8)
1+	24 (24.5)	16 (21.6)
2+	9 (9.2)	8 (10.8)
3+	39 (39.8)	26 (35.1)
Other	7 (7.1)	19 (25.7)
cerbB-2		
Negative	22 (22.4)	10 (13.5)
1+	19 (19.4)	13 (17.6)
2+	28 (28.6)	21 (28.4)
3+	22 (22.4)	11 (14.9)
Other	7 (7.1)	19 (25.7)
HER2 status		
Positive	26 (26.5)	16 (21.6)
Negative	65 (66.3)	39 (52.7)
Other	7 (7.1)	19 (25.7)
Ki-67 (%)	34.0±25.0	28.1±19.7
ADC value	0.88±0.25	0.83±0.20

Data are presented as mean ± SD or n (%). Other means that information absence or other types. SLN, sentinel lymph node; ER, estrogen receptor; PR, progesterone receptor; HER2, human epidermal growth factor receptor 2; ADC, apparent diffusion coefficient; SD, standard deviation.

validation was used to evaluate the model. Specifically, each subset (138 patients) was randomly divided into 10 folds, where nine folds (124 patients) were used to develop prediction model and the rest one (14 patients) was used to evaluate the model in sequence. The patients with SLN metastasis and non-SLN metastasis were labeled as 1 and 0, respectively. The ratio of SLN metastasis to non-SLN metastasis was the same in all subsets.

Imaging data acquisition

MRI was performed by using a 1.5-T MR imager (Achieva 1.5 T, Philips Healthcare, Best, Netherlands) equipped with a 4-channel SENSE breast coil. The diffusion-weighted (DW) images were acquired by single-shot spin-echo echo-planar imaging (EPI) and recorded by the picture archiving and communication system (PACS). The data acquisition parameters were as follows: resolution, 200 pixels × 196 pixels; field of view, 300×300 mm²; time of repetition/time of echo (TR/TE), 5,065/66 ms; slice thickness, 5 mm; slice gap, 1 mm; b values, 0 and 1,000 s/mm².

ROI segmentation

Segmentation of ROIs is required before quantitative feature extraction. The DWI Digital Imaging and Communications in Medicine (DICOM) images that had been archived in the PACS were transmitted to the radiologists without any pathological information and preprocessing. ITKSNAP 3.6 (ITK-SNAP 3.xTeam) was used by the radiologists for three-dimensional (3D) manual segmentation. Specifically, the radiologists first delineated the margin of tumor at each transverse plane, covered the whole tumor gradually, and repeated the above-mentioned procedure slice by slice. An example of segmentation is shown in the upper left of *Figure 1*. All manual segmentation was performed by a radiologist with 15 years of experience and was validated by a senior radiologist with 20 years of experience. A total of two radiologists involved in this work. And a radiologist with 15 years of experience performed manual segmentation, followed by a senior radiologist with 20 years of experience to validate and fine-tune the segmented results.

Image preprocessing and feature extraction

The preprocessing of ROIs is necessary, because the DWI

Table 2 Setting of different parameters in feature extraction

Parameters name	Values	Number of parameters
Wavelet band-pass filtering	Weight = [1/2, 2/3, 1, 3/2, 2]	5
Isotropic voxel size	Scale = {in-pR, 1, 2, 3, 4, 5}	6
Quantization algorithm	Quan algorithm = {Equal, Lloyd}	2
Number of gray levels	Ng [†] = [8, 16, 32, 64]	4

[†], Ng denotes gray levels respectively. in-pR, initial in-plane resolution.

images of different patients have different scan parameters (31,32). In the current study, a series of preprocessing methods were preformed, including: (I) wavelet bandpass filtering, aiming to denoise the noise in ROIs and focus on different bandwidth information, and the operator was performed by setting different weights to the bandpass or sub-bands of the ROIs in the wavelet domain; (II) isotropic resampling, aiming to keep rotation invariance and normalize the pixel and thickness, and the operator was carried out by cube interpolation to an appropriate resolution; and (III) quantization of gray level, aiming to normalize the different gray level of images affecting feature extraction, and the operator was performed by using equal-probability and Lloyd-Max quantization algorithms (33).

A series of texture and non-texture features were extracted from ROIs. Texture feature extraction was based on statistical distributions, including: (I) global features [dimension (D) =3], describe the histogram distribution of the ROIs intensity; (II) gray-level co-occurrence matrix (GLCM, D =9), depicting the statistical interrelationships between voxels of ROIs; (III) gray-level run-length matrix (GLRLM, D =13) and gray-level size zone matrix (GLSZM, D =13), computing the statistical interrelationship of neighboring voxels along a longitudinal run and the statistical distribution of similar and dissimilar regions; and (IV) neighborhood gray-tone difference matrix (NGTDM, D =5), quantifying the spatial interrelationship of neighboring voxels between adjacent image planes (34,35). Notably, the same preprocessing procedure with different parameters resulted in different features. As shown in *Table 2*, different parameters were used in the same procedure to enrich the texture features. Finally, $(3+9+13+13+5) \times (5 \times 6 \times 2 \times 4) = 10,320$ enhanced texture

features were obtained.

In addition, non-texture features were extracted to depict intuitional and simple image information, including: (I) volume, computed by the number of voxels in the ROIs multiplied by the dimension of voxels; (II) size, obtained by measuring the longest diameter of ROI; (III) solidity, the ratio of the number of voxels in the ROIs to the number of voxels in the 3D convex hull of the ROIs; and (IV) eccentricity, obtained by measuring the eccentricity of the ellipsoid that best fits the ROIs. All used features in our work are listed in *Table 3*. Totally, 10,320 texture features and four non-texture features were extracted from ROIs. Afterward, a linear normalization operator minimum-maximum method was used to eliminate the magnitude of features and negative effects of large magnitude difference.

Establishment of the optimal predictive model for SLN metastasis

As shown in *Figure 1*, the predictive model for SLN metastasis also included feature selection and classification modeling.

Feature selection methods

Feature selection can efficiently improve the performance of classification by eliminating redundant and irrelevant features. In general, feature selection methods are classified into three categories, namely, filter, wrapper, and embedded methods (36,37). Filter methods rank all the features in terms of their relevance scores based on their correlations with the class label, and choose an appropriate feature subset. Wrapper methods directly search for the feature subset with the optimal predictive performance for a given classification method. Embedded methods perform feature selection during classifier training to select stable and sparse features based on some strategies such as bootstrap and regularization. To compare different feature selection methods, 24 representative methods [including Las Vegas wrapper (LVW), sequential forward floating selection (SFFS), minimum redundancy maximum relevance (MRMR), and so on] were selected from the three categories. The abbreviations of all feature selection methods and their category are listed in *Table 4*.

Classification methods

Different classification methods with various complexity affect the performance of model directly. Therefore, 11 classifications methods [including boosting (BST), decision

Table 3 Summary of texture feature extraction

Type of texture	Parameters
First order	
Global (D [†] =3)	Variance (No. 1), skewness (No. 2), kurtosis (No. 3)
Second order	
GLCM (D =9)	Energy (No. 4), contrast (No. 5), correlation (No. 6), homogeneity (No. 7), variance (No. 8), sum average (No. 9), entropy (No. 10), dissimilarity (No. 11), auto-correlation (No. 12)
High order	
GLRLM (D =13)	Short run emphasis (No. 13), long run emphasis (No. 14), gray-level nonuniformity (No. 15), run-length nonuniformity (No. 16), run percentage (No. 17), low gray-level run emphasis (No. 18), high gray-level run emphasis (No. 19), short run low gray-level emphasis (No. 20), short run high gray-level emphasis (No. 21), long run low gray-level emphasis (No. 22), long run high gray-level emphasis (No. 23), gray-level variance (No. 24), run-length variance (No. 25)
GLZSM (D =13)	Small zone emphasis (No. 26), large zone emphasis (No. 27), gray-level nonuniformity (No. 28), zone-size nonuniformity (No. 29) zone percentage (No.30), low gray-level zone emphasis (No. 31), high gray-level zone emphasis (No. 32), small zone low gray-level emphasis (No. 33), small zone high gray-level emphasis (No. 34), large zone low gray-level emphasis (No. 35), large zone high gray-level emphasis (No. 36), gray-level variance (No. 37), zone-size variance (No. 38)
NGTDM (D =5)	Coarseness (No. 39), contrast (No. 40), busyness (No. 41), complexity (No. 42), strength (No. 43)

[†], D denotes dimension of feature space. The number inside parenthesis denotes the feature number. GLCM, gray-level co-occurrence matrix; GLRLM, gray-level run-length matrix; GLZSM, gray-level size zone matrix; NGTDM, neighborhood gray-tone difference matrix.

tree (DT), random forest (RF), etc.] were extensively investigated. The abbreviations of all classification methods are also listed in *Table 4*. Most parameters in the classification methods were selected by 10-fold cross-validation in each training set, whereas others were chosen based on fine-tuning default parameters in all methods.

Optimal feature selection—classification combination analysis

The optimal combination of feature selection and classification methods in terms of their predictive performance and stability were first identified. The feature selection and classification were then compared independently to explore predictive performance of feature selection and classification method separately.

Predictive performances of feature selection-classification combinations

In this paper, the predictive performances of the feature selection and classification methods were compared by cross-combination. The features selected by each feature selection method were subsequently transferred to the classification method. The predictive performance of each combination for each subset was evaluated using area under

the curve (AUC) and ACC. The aforementioned process was repeated to the 50 subsets. The final performance of any combination was assessed in terms of average values of AUC and ACC over 50 subsets.

Stability of feature selection-classification combinations

The stability of combination of feature selection and classification method is mainly caused by the perturbation of random dataset partition. In addition to perturbation of dataset, choice of feature selection and classification method is also an important factor for stability of feature selection and classification category. To quantify stability, the relative standard deviation (RSD) was used to assess the feature selection and classification methods. RSD is the absolute value of the ratio of standard deviation (SD) to average, and it is defined as:

$$RSD = \frac{\sigma_{AUC}}{\mu_{AUC}} \times 100 \quad [1]$$

where σ_{AUC} and μ_{AUC} are the SD and average of AUC, respectively. It indicates that a lower value means more stability. For each combination of feature selection and classification method, AUC_{subset} was first obtained over 10-fold at each subset, and then σ_{AUC} and μ_{AUC} were computed based on AUC_{subset} over the 50 subsets.

Table 4 The list of all feature selection and classification methods used in our work

Feature selection method acronym	Feature selection method name	Classification method acronym	Classification method name
LVW [†]	Las Vegas wrapper	BAG	Bagging
SFFS [†]	Sequential forward floating selection	BAYES	Naive bayes
SFS [†]	Sequential forward selection	BST	Boosting
RF [‡]	Random forest	L-DA	Linear discriminant analysis
RFE [‡]	Recursive feature elimination	DT	Decision tree
L^1 -SVM [‡]	L^1 regularization based on SVM	GLM	Generalized linear model
L^2 -SVM [‡]	L^2 regularization based on SVM	K-NN	k-nearest neighbor
CHSQ [§]	Chi-square score	SVM	Support vector machine
CIFE [§]	Conditional infomax feature extraction	MARS	Multi-adaptive regression splines
CMIM [§]	Conditional mutual information maximization	PLSR	Partial least squares regression
DISR [§]	Double input symmetric relevance	RF	Random forest
DC [§]	Distance correlation		
FSCR [§]	Fisher score		
GINI [§]	Gini index		
ICAP [§]	Interaction capping		
ILFS [§]	Infinite latent feature selection		
JMI [§]	Joint mutual information		
LS [§]	Laplacian score		
MIFS [§]	Mutual information feature selection		
MIM [§]	Mutual information maximization		
MRMR [§]	Minimum redundancy maximum relevance		
RELF [§]	Relieff		
SIS [§]	Sure independence screening		
TSCR [§]	T-score		

[†], the feature selection method from wrapper category; [‡], the feature selection method from embedded category; [§], the feature selection method from filter category. And more details can refer to (34,35).

Obviously, combination of feature selection and classification methods with the highest prediction performance and the best stability is the optimal model for prediction of SLN metastasis in breast cancer.

Performance analysis based on feature selection and classification method respectively

The predictive performance of feature selection and classification methods were further compared separately.

For each feature selection method, the average AUC and ACC were computed over the 11 classification methods. Meanwhile, the stability of feature selection methods and classification methods were investigated separately. The RSD of each feature selection method and classification method was also calculated. As to each feature selection method, σ_{AUC} and μ_{AUC} were yielded over the 11 classification methods. Correspondingly, to each classification method, σ_{AUC} and μ_{AUC} were yielded over the 24 feature selection methods.

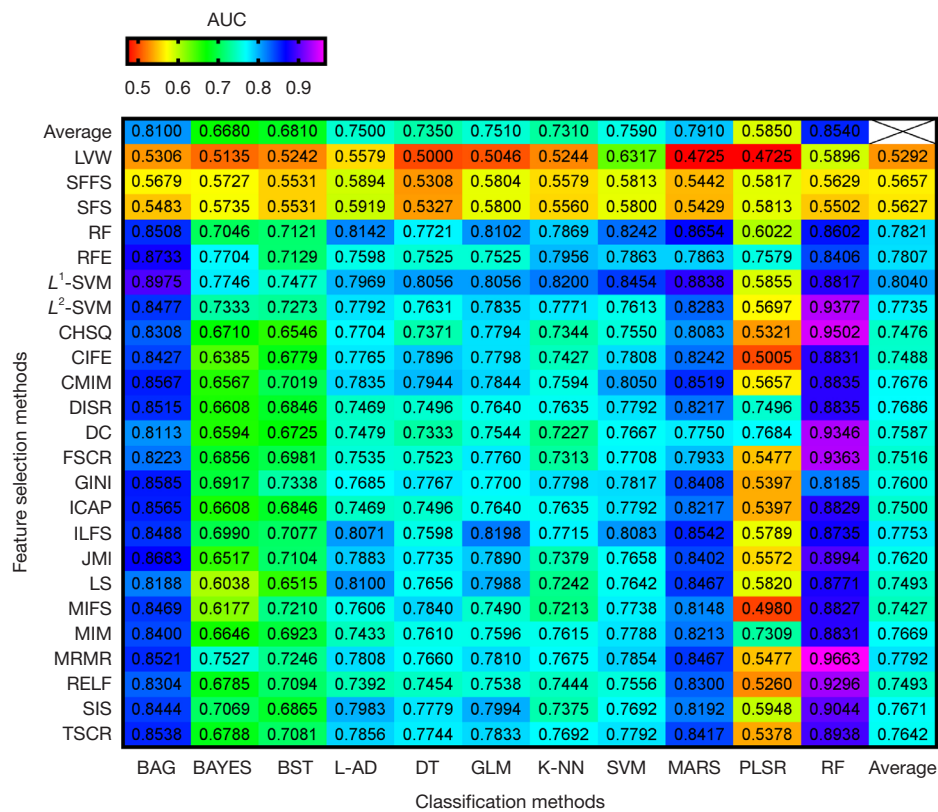


Figure 2 Heatmap depicting the predictive performance (AUC) of feature selection (in rows) and classification (in columns) methods. It depicts the mean AUC of any combination over 50 datasets. The top and the far right of figure shows the average AUC of feature selection and classification method, separately. The abbreviations of feature selection and classification methods were defined in Table 4. AUC, area under curve.

Statistical analysis

All the analyses were implemented using R software 3.4.2 (R Core Team, Vienna, Austria) and MATLAB 2016b (MathWorks, Natick, MA, USA).

Results

Predictive performances of feature selection-classification combinations

AUC and ACC were used to quantify the predictive performances of the cross-combinations of 24 feature selection and 11 classification methods. In total, 264 different combinations were assessed in this study. Figures 2,3 showed the specific AUC and ACC values. The results show that MRMR + RF exhibited the optimal predictive performance [(AUC: 0.97±0.03; range: 0.95–1.00) and (ACC: 0.89±0.05; range: 0.86–0.93)], followed by chi-

square score (CHSQ) + RF [(AUC: 0.95±0.04; range: 0.94–0.98) and (ACC: 0.89±0.05; range: 0.86–0.93)] and L²-support vector machine (L²-SVM) + RF [(AUC: 0.94±0.05; range: 0.91–0.98) and (ACC: 0.87±0.05; range: 0.86–0.93)]. The confusion matrix of three feature selection-classification combinations with good model performance (i.e., MRMR + RF, CHSQ + RF, and L²-SVM + RF) are shown in Figure 4, which contained the testing results in all subsets. The three methods could correctly predict most of the positive and negative classes, and the positive samples were relatively easier to classify compared with the negative ones.

Stability of the feature selection-classification combinations

The RSD was computed to assess the stability of the different combination models. As Figure 5 shown, MRMR + RF exhibited the best stability (stability: 2.94), followed by

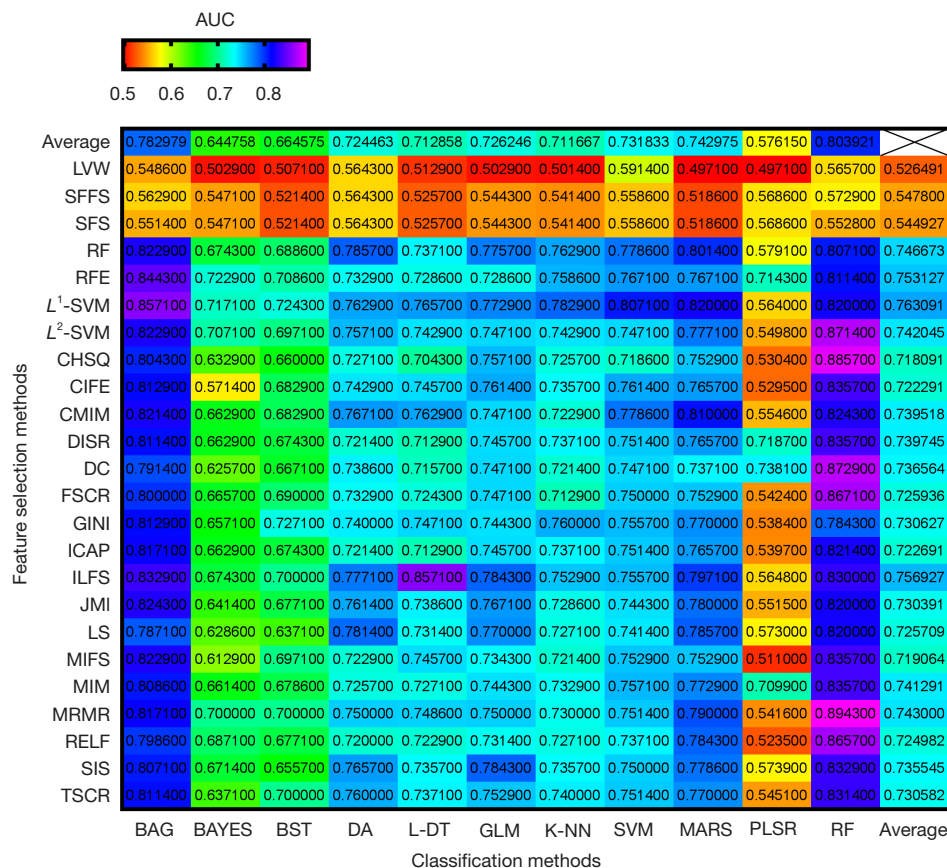


Figure 3 Heatmap depicting the predictive performance (ACC) of feature selection (in rows) and classification (in columns) methods. It depicts the mean ACC of any combination over 50 datasets. The top and the far right of figure shows the average ACC of feature selection and classification method, separately. The abbreviations of feature selection and classification methods were defined in *Table 4*. ACC, accuracy.

DC + RF (stability: 3.96) and CHSQ + RF (stability: 3.97).

Performance analysis based on feature selection and classification method respectively

For the average performance of prediction made by feature selection and classification method separately, as the top and the far right of *Figures 2,3* shown, L¹-SVM selection methods [(AUC: 0.80±0.08; range: 0.59–0.90) and (ACC: 0.76±0.07; range: 0.56–0.86)] and RF classifier [(AUC: 0.85±0.11; range: 0.55–0.97) and (ACC: 0.80±0.09; range: 0.55–0.89)] showed the best predictive performance among their respective categories. As to the average stability made by feature selection methods and classification methods separately, it can be observed from the top and the far right of *Figure 5* that SFFS (stability: 3.04) and RF (stability:

8.84) showed the optimal stability among their respective categories. Overall, in addition to the RF classifier, bootstrap aggregating (BAG) was also a well-performed ensemble method [(AUC: 0.81±0.10; range: 0.53–0.89), (ACC: 0.78±0.09; range: 0.54–0.85), and (stability: 9.36)], followed by multi-adaptive regression splines (MARS) [(AUC: 0.79±0.10; range: 0.47–0.88), (ACC: 0.74±0.09; range: 0.49–0.82), and (stability: 9.59)], while SVM, generalize linear model (GLM), linear discriminant analysis (L-DA), k-nearest neighbor (KNN), and DT [(average AUC range: 0.73–0.76), (average ACC range: 0.71–0.73), and (stability range: 10.04–10.43)] obtained similar model performance. In contrast, binary search tree (BST), naive bayes (BAYES), and partial least squares regression (PLSR) [(average AUC range: 0.59–0.68), (average ACC range: 0.58–0.66), and (stability range: 11.21–13.64)] had relatively

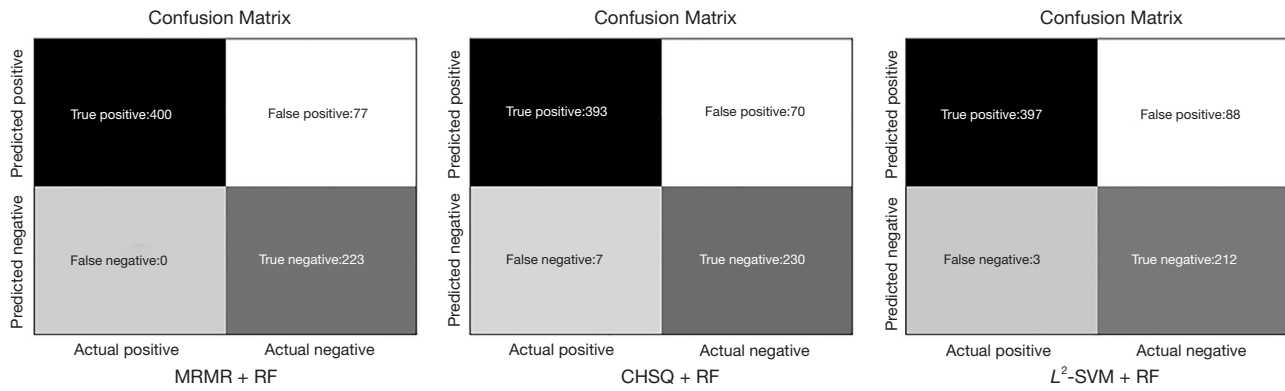


Figure 4 Confusion matrix of the promising feature selection-classification combinations (i.e., MRMR + RF, CHSQ + RF, and L²-SVM + RF). It depicts the numbers of true positive, false positive, false negative, and true negative samples in the testing stage over all 50 subsets. MRMR, minimum redundancy maximum relevance; RF, random forest; CHSQ, chi-square score; SVM, support vector machine.

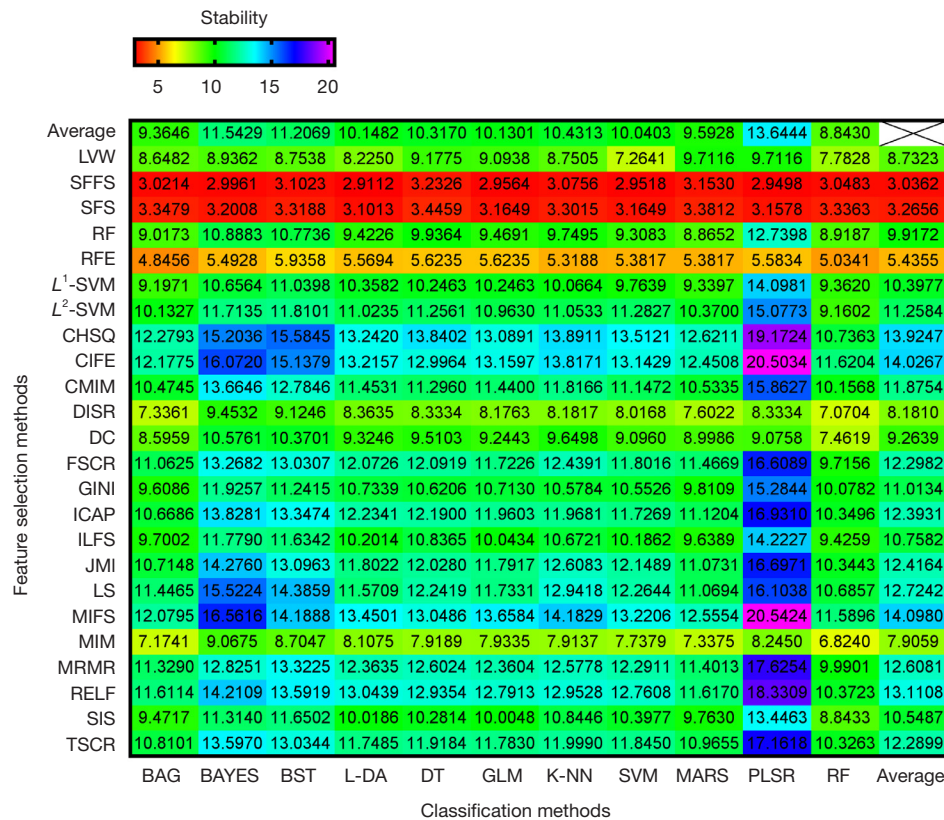


Figure 5 Heatmap depicting the stability of feature selection (in rows) and classification (in columns) methods. It depicts the mean stability of any combination over 50 datasets. The top and the far right of figure shows the average stability of feature selection and classification method, separately. The abbreviations of feature selection and classification methods were defined in Table 4.

Table 5 The list of top 5 contributing factors in each feature selection method

Feature selection method acronym	Feature 1	Feature 2	Feature 3	Feature 4	Feature 5
LVW [†]	No. 24 [209]	No. 30 [15]	No. 14 [52]	No. 37 [237]	No. 43 [36]
SFFS [†]	No. 26 [39]	No. 26 [63]	No. 26 [85]	No. 32 [110]	No. 26 [157]
SFS [†]	No. 26 [154]	No. 26 [14]	No. 26 [10]	No. 32 [5]	No. 26 [49]
RF [‡]	No. 43 [73]	No. 34 [138]	No. 31 [142]	No. 27 [12]	No. 30 [14]
RFE [‡]	No. 34 [89]	No. 28 [17]	No. 31 [165]	No. 34 [173]	No. 28 [225]
L^1 -SVM [‡]	No. 1 [241]	No. 38 [1]	No. 34 [173]	No. 33 [105]	No. 33 [14]
L^2 -SVM [‡]	No. 29 [229]	No. 34 [89]	No. 31 [165]	No. 26 [229]	No. 28 [17]
CHSQ [§]	No. 36 [142]	No. 36 [71]	No. 36 [23]	No. 26 [98]	No. 29 [146]
CIFE [§]	No. 35 [8]	No. 35 [47]	No. 35 [24]	No. 35 [95]	No. 35 [96]
CMIM [§]	No. 12 [126]	No. 43 [169]	No. 22 [19]	No. 20 [24]	No. 41 [27]
DISR [§]	No. 12 [126]	No. 10 [150]	No. 34 [104]	No. 16 [200]	No. 13 [200]
DC [§]	No. 38 [14]	No. 38 [62]	No. 25 [105]	No. 38 [110]	No. 28 [177]
FSCR [§]	No. 26 [105]	No. 26 [159]	No. 26 [14]	No. 29 [111]	No. 29 [159]
GINI [§]	No. 12 [1]	No. 10 [3]	No. 34 [2]	No. 16 [1]	No. 13 [4]
ICAP [§]	No. 15 [126]	No. 15 [150]	No. 9 [104]	No. 28 [200]	No. 19 [200]
ILFS [§]	No. 28 [5]	No. 29 [5]	No. 30 [5]	No. 31 [5]	No. 32 [5]
JMI [§]	No. 23 [143]	No. 32 [56]	No. 32 [72]	No. 9 [143]	No. 23 [144]
LS [§]	No. 30 [128]	No. 30 [31]	No. 30 [72]	No. 30 [120]	No. 30 [135]
MIFS [§]	No. 35 [8]	No. 35 [24]	No. 35 [32]	No. 35 [40]	No. 35 [47]
MIM [§]	No. 12 [126]	No. 10 [150]	No. 34 [104]	No. 16 [200]	No. 13 [200]
MRMR [§]	No. 26 [77]	No. 38 [110]	No. 26 [207]	No. 27 [210]	No. 29 [54]
RELF [§]	No. 34 [61]	No. 19 [34]	No. 32 [42]	No. 34 [10]	No. 29 [206]
SIS [§]	No. 26 [159]	No. 29 [159]	No. 26 [105]	No. 26 [14]	No. 26 [63]
TSCR [§]	No. 35 [196]	No. 35 [204]	No. 35 [212]	No. 35 [228]	No. 35 [236]
Total	No. 26	No. 35	No. 34	No. 30	No. 29

[†], the feature selection method from wrapper category; [‡], the feature selection method from embedded category; [§], the feature selection method from filter category. The bottom row shows five most common features among all feature selection methods. The number out of square bracket denotes the feature number in *Table 3*. The number inside square bracket denotes combination of parameters in *Table 2*. The abbreviations of feature selection methods were defined in *Table 4*.

inferior results.

Contributing features based on feature selection methods

The top 5 contributing features obtained by each feature selection method are shown in *Table 5*. All the best performed contributing features were texture features,

probably because the non-texture features did not contain as much abundant information as the texture ones. The five most common features among all 24 feature selection methods were small zone emphasis (No. 26), large zone low gray-level emphasis (No. 35), small zone high gray-level emphasis (No. 34), zone percentage (No. 30), and zone-size nonuniformity (No. 29).

Discussion

Key findings

Recent studies have proven that SLNB is an alternative method for ALN metastasis detection (7,8,10). However, biopsy can bring discomfort and injury to patients, such as pain, bleeding, infection, etc. (11,12). Therefore, it is of great importance to develop a non-invasive SLN metastasis detection method. So far, machine-learning based approaches have been applied in medical image-based auxiliary diagnostic studies for varied cancers (20,23,34), histology (36,37), survival prediction (24,38), and so on. In this study, a machine learning framework for preoperative prediction of SLN metastasis in breast cancer was proposed with assessments of different selection and classification model. The findings suggested an optimal model of combination of MRMR feature selection and RF classification methods and showed a relatively high efficiency for prediction of SLN metastasis in breast cancer.

Strengths and limitations

The one limitation of our work is that our proposed model is lack of large and independent external validation. Therefore, we used 10-fold cross-validation to assess the performance of model, which is an efficient way to decrease the variance of performance due to random dataset partition, especially for the limited number of patients. On the one hand, multicenter and prospective patient collection should be proceeded; on the other hand, a more proper way to solve the limited data problem deserves further investigation. Another possible limitation of our study is that the effect of magnetic field inhomogeneity is not considered. And the DW image is sensitive to magnetic field inhomogeneity which might result in bias for the results.

Comparison with similar researches

The promising prediction performance partly benefited from the feature selection method that decreased the dimension of feature space by identifying a set of the most contributing features. During the feature selection process, the redundancy between features and the risk of model overfitting partly decreased. In addition, classification methods play a leading role based on the given feature set after feature selection, and classification methods from different families have their own operational mechanisms

with discrepant performances (39).

Explanations of findings

The results of our experiments showed that the ensemble methods such as RF classifier and BAG could obtained outstanding performance, followed by MARS, while SVM, GLM, L-DA, KNN, and DT achieved general results. Meanwhile, BST, BAYES, and PLSR got inferior performance compared with others. The possible confounding factors leading to inferior performance might be that BST, BAYES, and KNN are relatively sensitive to noise and data distribution (40-42), PLSR and GLM relied on linear assumption and could not handle nonlinear problem, MARS, L-DA and DT were likely to suffer from overfitting (43,44), SVM was easily impacted by the selection of kernel function (45). Although RF and BAG might also be affected by noise interference and required more computational power, they combined multiple uncorrelated base models and made decision based on the majority of votes that helped improve the ACC (46), thus these two models were more suitable for the current study. It is worth noting that, from the machine learning point of view, different combinations of feature selection and classification methods would lead to differences in performance, particularly for a high-dimensional dataset. The current study widely studied and compared the performances and stability of cross-combinations of 24 typical feature selection and 11 classification methods from different categories. On the basis of predictive performance and stability for preoperative prediction of SLN metastasis in breast cancer, our study offered evidence that the combination MRMR + RF is the optimal model than other combinations. MRMR is a filter method based on mutual information. It selects a feature set with minimum redundancy and maximum relevance (47). The results suggested that the enhanced features might have more redundancy. RF classifier is a supervised learning classification method (39). This classifier consists of an ensemble of tree predictors, with each tree depending on the values of a random vector sampled independently. RF has ability to expose the hidden linear or nonlinear relationship between the feature and target. Its favorable performance has also been confirmed in several previous studies (20,34,48).

Performance for the categories of feature selection and classification method was also explored separately in this study. The results showed that L^1 -SVM and SFFS had the

best average predictive performance and the stability among all feature selection methods, respectively. RF and SVM showed the best average predictive performance and the stability among all classification methods (49), respectively. These results indicated that L^1 -SVM and SFFS has better robustness for feature selection in general, and RF and SVM are better selection of classifiers compared with other approaches. In general, for similar tasks, such as metastasis of other lymph node, priority can be given to the above feature selection methods and classifiers.

Implications and actions needed

Therefore, more collection of magnetic field inhomogeneity of DW images should be included in future research. In addition, our work only identified the combination of traditional methods with a relatively high predictive and stable performance for preoperative prediction of SLN metastasis in breast cancer. In the future, we will study the influences of different parameters in image acquisition and feature extraction and use more complex machine learning methods, including deep learning methods based on patch strategy (34).

Conclusions

In conclusion, an optimal machine-learning model for preoperative prediction of SLN metastasis in breast cancer was established based on the image features of MRI. The combination of MRMR and RF suggested the best predictive efficiency. It could facilitate clinical prediction of SLN metastasis for patients with breast cancer.

Acknowledgments

Funding: This work was supported by the National Natural Science Foundation of China (Nos. 61671230 and 31271067), the Science and Technology Program of Guangdong Province (No. 2017A020211012), the Guangdong Provincial Key Laboratory of Medical Image Processing (No. 2014B030301042), and the Science and Technology Program of Guangzhou (No. 201607010097).

Footnote

Reporting Checklist: The authors have completed the TRIPOD reporting checklist. Available at <https://tcr.amegroups.com/article/view/10.21037/tcr-22-2534/rc>

Data Sharing Statement: Available at <https://tcr.amegroups.com/article/view/10.21037/tcr-22-2534/dss>

Conflicts of Interest: All authors have completed the ICMJE uniform disclosure form (available at <https://tcr.amegroups.com/article/view/10.21037/tcr-22-2534/coif>). The authors have no conflicts of interest to declare.

Ethical Statement: The authors are accountable for all aspects of the work in ensuring that questions related to the accuracy or integrity of any part of the work are appropriately investigated and resolved. This study does not need Institutional Review Board (IRB) approval due to the purpose of retrospective study and was conducted in accordance with the Declaration of Helsinki (as revised in 2013). The individual consent for this retrospective analysis was waived.

Open Access Statement: This is an Open Access article distributed in accordance with the Creative Commons Attribution-NonCommercial-NoDerivs 4.0 International License (CC BY-NC-ND 4.0), which permits the non-commercial replication and distribution of the article with the strict proviso that no changes or edits are made and the original work is properly cited (including links to both the formal publication through the relevant DOI and the license). See: <https://creativecommons.org/licenses/by-nc-nd/4.0/>.

References

1. Sung H, Ferlay J, Siegel RL, et al. Global Cancer Statistics 2020: GLOBOCAN Estimates of Incidence and Mortality Worldwide for 36 Cancers in 185 Countries. *CA Cancer J Clin* 2021;71:209-49.
2. Chlebowski RT, Manson JE, Anderson GL, et al. Estrogen plus progestin and breast cancer incidence and mortality in the Women's Health Initiative Observational Study. *J Natl Cancer Inst* 2013;105:526-35.
3. Qiu PF, Liu JJ, Wang YS, et al. Risk factors for sentinel lymph node metastasis and validation study of the MSKCC nomogram in breast cancer patients. *Jpn J Clin Oncol* 2012;42:1002-7.
4. Pinheiro DJ, Elias S, Nazário AC. Axillary lymph nodes in breast cancer patients: sonographic evaluation. *Radiol Bras* 2014;47:240-4.
5. Xu Z, Ding Y, Zhao K, et al. MRI characteristics of breast edema for assessing axillary lymph node burden in early-stage breast cancer: a retrospective bicentric study. *Eur*

- Radiol 2022;32:8213-25.
6. Kim T, Giuliano AE, Lyman GH. Lymphatic mapping and sentinel lymph node biopsy in early-stage breast carcinoma: a metaanalysis. *Cancer* 2006;106:4-16.
 7. Lyman GH, Giuliano AE, Somerfield MR, et al. American Society of Clinical Oncology guideline recommendations for sentinel lymph node biopsy in early-stage breast cancer. *J Clin Oncol* 2005;23:7703-20.
 8. Veronesi U, Paganelli G, Viale G, et al. A randomized comparison of sentinel-node biopsy with routine axillary dissection in breast cancer. *N Engl J Med* 2003;349:546-53.
 9. Liu P, Tan J, Song Y, et al. The Application of Magnetic Nanoparticles for Sentinel Lymph Node Detection in Clinically Node-Negative Breast Cancer Patients: A Systemic Review and Meta-Analysis. *Cancers (Basel)* 2022;14:5034.
 10. Kimura F, Yoshimura M, Koizumi K, et al. Radiation exposure during sentinel lymph node biopsy for breast cancer: effect on pregnant female physicians. *Breast Cancer* 2015;22:469-74.
 11. Wilke LG, McCall LM, Posther KE, et al. Surgical complications associated with sentinel lymph node biopsy: results from a prospective international cooperative group trial. *Ann Surg Oncol* 2006;13:491-500.
 12. Sugden EM, Rezvani M, Harrison JM, et al. Shoulder movement after the treatment of early stage breast cancer. *Clin Oncol (R Coll Radiol)* 1998;10:173-81.
 13. Chen JY, Chen JJ, Yang BL, et al. Predicting sentinel lymph node metastasis in a Chinese breast cancer population: assessment of an existing nomogram and a new predictive nomogram. *Breast Cancer Res Treat* 2012;135:839-48.
 14. Nottegar A, Veronese N, Senthil M, et al. Extra-nodal extension of sentinel lymph node metastasis is a marker of poor prognosis in breast cancer patients: A systematic review and an exploratory meta-analysis. *Eur J Surg Oncol* 2016;42:919-25.
 15. La Verde N, Biagioli E, Gerardi C, et al. Role of patient and tumor characteristics in sentinel lymph node metastasis in patients with luminal early breast cancer: an observational study. *Springerplus* 2016;5:114.
 16. Viale G, Zurrida S, Maiorano E, et al. Predicting the status of axillary sentinel lymph nodes in 4351 patients with invasive breast carcinoma treated in a single institution. *Cancer* 2005;103:492-500.
 17. Ozemir IA, Orhun K, Eren T, et al. Factors affecting sentinel lymph node metastasis in Turkish breast cancer patients: Predictive value of Ki-67 and the size of lymph node. *Bratisl Lek Listy* 2016;117:436-41.
 18. Omoto K, Matsunaga H, Take N, et al. Sentinel node detection method using contrast-enhanced ultrasonography with sonazoid in breast cancer: preliminary clinical study. *Ultrasound Med Biol* 2009;35:1249-56.
 19. Lambin P, Leijenaar RTH, Deist TM, et al. Radiomics: the bridge between medical imaging and personalized medicine. *Nat Rev Clin Oncol* 2017;14:749-62.
 20. Zhang B, He X, Ouyang F, et al. Radiomic machine-learning classifiers for prognostic biomarkers of advanced nasopharyngeal carcinoma. *Cancer Lett* 2017;403:21-7.
 21. Chen T, Ning Z, Xu L, et al. Radiomics nomogram for predicting the malignant potential of gastrointestinal stromal tumours preoperatively. *Eur Radiol* 2019;29:1074-82.
 22. Cunha GM, Fowler KJ. Automated Liver Segmentation for Quantitative MRI Analysis. *Radiology* 2022;302:355-6.
 23. Li H, Zhu Y, Burnside ES, et al. Quantitative MRI radiomics in the prediction of molecular classifications of breast cancer subtypes in the TCGA/TCIA data set. *NPJ Breast Cancer* 2016;2:16012-.
 24. Zhou M, Leung A, Echeagaray S, et al. Non-Small Cell Lung Cancer Radiogenomics Map Identifies Relationships between Molecular and Imaging Phenotypes with Prognostic Implications. *Radiology* 2018;286:307-15.
 25. Kuo MD, Jamshidi N. Behind the numbers: Decoding molecular phenotypes with radiogenomics--guiding principles and technical considerations. *Radiology* 2014;270:320-5.
 26. Gillies RJ, Kinahan PE, Hricak H. Radiomics: Images Are More than Pictures, They Are Data. *Radiology* 2016;278:563-77.
 27. Bolón-Canedo V, Sánchez-Marono N, Alonso-Betanzos A. A review of feature selection methods on synthetic data. *Knowl Inf Syst* 2013;34:483-519.
 28. Bolón-Canedo V, Sánchez-Marono N, Alonso-Betanzos A, et al. A review of microarray datasets and applied feature selection methods. *Information Sciences* 2014;282:111-35.
 29. Tan KM, London P, Mohan K, et al. Learning Graphical Models With Hubs. *J Mach Learn Res* 2014;15:3297-331.
 30. Haury AC, Gestraud P, Vert JP. The influence of feature selection methods on accuracy, stability and interpretability of molecular signatures. *PLoS One* 2011;6:e28210.
 31. Ganeshan B, Goh V, Mandeville HC, et al. Non-small cell lung cancer: histopathologic correlates for texture parameters at CT. *Radiology* 2013;266:326-36.

32. Lv W, Yuan Q, Wang Q, et al. Robustness versus disease differentiation when varying parameter settings in radiomics features: application to nasopharyngeal PET/CT. *Eur Radiol* 2018;28:3245-54.
33. Max J. Quantizing for minimum distortion. *IRE Trans Inf Theory* 1960;6:7-12.
34. Ning Z, Luo J, Li Y, et al. Pattern Classification for Gastrointestinal Stromal Tumors by Integration of Radiomics and Deep Convolutional Features. *IEEE J Biomed Health Inform* 2019;23:1181-91.
35. Vallières M, Freeman CR, Skamene SR, et al. A radiomics model from joint FDG-PET and MRI texture features for the prediction of lung metastases in soft-tissue sarcomas of the extremities. *Phys Med Biol* 2015;60:5471-96.
36. Spanhol FA, Oliveira LS, Petitjean C, et al. A Dataset for Breast Cancer Histopathological Image Classification. *IEEE Trans Biomed Eng* 2016;63:1455-62.
37. Hamidinekoo A, Denton E, Rampun A, et al. Deep learning in mammography and breast histology, an overview and future trends. *Med Image Anal* 2018;47:45-67.
38. Cheng J, Zhang J, Han Y, et al. Integrative Analysis of Histopathological Images and Genomic Data Predicts Clear Cell Renal Cell Carcinoma Prognosis. *Cancer Res* 2017;77:e91-e100.
39. Mohan K, London P, Fazel M, et al. Node-Based Learning of Multiple Gaussian Graphical Models. *J Mach Learn Res* 2014;15:445-88.
40. Bootkrajang J, Kabán A. Boosting in the presence of label noise. arXiv:1309.6818 [Preprint]. 2013. Available online: <https://arxiv.org/abs/1309.6818>
41. Jadhav SD, Channe HP. Comparative study of K-NN, naive Bayes and decision tree classification techniques. *International Journal of Science and Research (IJSR)* 2016;5:1842-5.
42. Zhang S. Cost-sensitive KNN classification. *Neurocomputing* 2020;391:234-42.
43. Bateni SM, Vosoughifar HR, Truce B, et al. Estimation of clear-water local scour at pile groups using genetic expression programming and multivariate adaptive regression splines. *J Waterw Port Coast Ocean Eng* 2019;145:04018029.
44. Luo D, Ding C, Huang H. Linear discriminant analysis: New formulations and overfit analysis. In: *Proceedings of the AAAI Conference on Artificial Intelligence*. 2011;25:417-22.
45. Hussain M, Wajid SK, Elzaart A, et al. A comparison of SVM kernel functions for breast cancer detection. In: *2011 Eighth International Conference Computer Graphics, Imaging and Visualization*. IEEE; 2011:145-50.
46. Fawagreh K, Gaber MM, Elyan E. Random forests: from early developments to recent advancements. *Systems Science & Control Engineering: An Open Access Journal* 2014;2:602-9.
47. Peng H, Long F, Ding C. Feature selection based on mutual information: criteria of max-dependency, max-relevance, and min-redundancy. *IEEE Trans Pattern Anal Mach Intell* 2005;27:1226-38.
48. Parmar C, Grossmann P, Bussink J, et al. Machine Learning methods for Quantitative Radiomic Biomarkers. *Sci Rep* 2015;5:13087.
49. Fan J, Samworth R, Wu Y. Ultrahigh dimensional feature selection: beyond the linear model. *J Mach Learn Res* 2009;10:2013-38.

Cite this article as: Wang J, Gao X, Zhang S, Zhang Y. Machine-learning methods based on the texture and non-texture features of MRI for the preoperative prediction of sentinel lymph node metastasis in breast cancer. *Transl Cancer Res* 2023;12(12):3471-3485. doi: 10.21037/tcr-22-2534